


## RESEARCH ARTICLE

# Unmanned aircraft system advances health mapping of fragile polar vegetation

Zbyněk Malenovský<sup>1,2,3</sup>  | Arko Lucieer<sup>1</sup> | Diana H. King<sup>2</sup> | Johanna D. Turnbull<sup>2</sup> | Sharon A. Robinson<sup>2</sup>

<sup>1</sup>Surveying and Spatial Sciences Group, School of Land and Food, University of Tasmania, Hobart, Tas., Australia

<sup>2</sup>Centre for Sustainable Ecosystem Solutions, School of Biological Sciences, University of Wollongong, Wollongong, NSW, Australia

<sup>3</sup>Biospheric Sciences Laboratory, USRA/GESTAR, NASA Goddard Space Flight Center, Greenbelt, MD, USA

**Correspondence**

Zbyněk Malenovský  
Email: zbynek.malenovsky@gmail.com

**Funding information**

Australian Antarctic Division, Grant/Award Number: 4046 and 4361; Australian Research Council, Grant/Award Number: DP110101714

Handling Editor: Nicolas Lecomte

**Abstract**

1. Plants like mosses can be sensitive stress markers of subtle shifts in Arctic and Antarctic environmental conditions, including climate change. Traditional ground-based monitoring of fragile polar vegetation is, however, invasive, labour intensive and physically demanding. High-resolution multispectral satellite observations are an alternative, but even their recent highest achievable spatial resolution is still inadequate, resulting in a significant underestimation of plant health due to spectral mixing and associated reflectance impurities.
2. To resolve these obstacles, we have developed a new method that uses low-altitude unmanned aircraft system (UAS) hyperspectral images of sub-decimeter spatial resolution. Machine-learning support vector regressions (SVR) were employed to infer Antarctic moss vigour from quantitative remote sensing maps of plant canopy chlorophyll content and leaf density. The same maps were derived for comparison purposes from the WorldView-2 high spatial resolution (2.2 m) multispectral satellite data.
3. We found SVR algorithms to be highly efficient in estimating plant health indicators with acceptable root mean square errors (*RMSE*). The systematic *RMSE*s for chlorophyll content and leaf density were 3.5–6.0 and 1.3–2.0 times smaller, respectively, than the unsystematic errors. However, application of correctly trained SVR machines on space-borne multispectral images considerably underestimated moss chlorophyll content, while stress indicators retrieved from UAS data were found to be comparable with independent field measurements, providing statistically significant regression coefficients of determination (median  $r^2 = .50$ ,  $p_{t\text{ test}} = .0072$ ).
4. This study demonstrates the superior performance of a cost-efficient UAS mapping platform, which can be deployed even under the continuous cloud cover that often obscures optical high-altitude airborne and satellite observations. Antarctic moss vigour maps of appropriate resolution could provide timely and spatially explicit warnings of environmental stress events, including those triggered by climate change. Since our polar vegetation health assessment method is based on physical principles of quantitative spectroscopy, it could be adapted to other short-stature and fragmented plant communities (e.g. tundra grasslands), including alpine and desert regions. It therefore shows potential to become an operational component of any ecological monitoring sensor network.

**KEYWORDS**

Antarctic moss stress, chlorophyll content, effective leaf density, multispectral and hyperspectral remote sensing, quantitative imaging spectroscopy, relative plant vigour, satellite and airborne mapping, unmanned aircraft system, unmanned aerial vehicle

## 1 | INTRODUCTION

The polar regions are characterized by short-stature (ground hugging) cryptogamic vegetation (mosses, liverworts, lichens and algae) that occupies scattered ice-free Arctic and Antarctic habitats (Convey et al., 2014). This flora survives some of the most hostile conditions on Earth, exacerbated by the recent impacts of climate change and ozone depletion (Convey et al., 2009; Robinson & Erickson, 2015; Turner, Barrand, et al., 2014). Its life is a permanent balancing act between acquisition of life-sustaining resources and protection against potentially lethal disturbances. As such, these plant communities serve as critical markers of subtle, but essential spatial and temporal changes in polar terrestrial ecosystems (Bramley-Alves, Wanek, French, & Robinson, 2015; Clarke, Robinson, Hua, Ayre, & Fink, 2012; Newsham & Robinson, 2009; Royles et al., 2013). Regular and spatially representative monitoring of their health can provide us with a unique early warning system for environmental shifts (Brabyn, Green, Beard, & Seppelt, 2005; Guglielmin, Fratte, & Cannone, 2014; Robinson, Turnbull, & Lovelock, 2005; Turnbull & Robinson, 2009; Wasley, Robinson, Lovelock, & Popp, 2006), for example arctic greening and subsequent browning (Phoenix & Bjerke, 2016). Traditional field investigation is, however, physically and methodologically challenging (Wasley et al., 2012), requiring several people to perform invasive manual sampling and *in-situ* measurements during short summer seasons characterized by rapid weather changes. A fast and efficient remote sensing method, which eliminates these hurdles while providing health assessment with comparable accuracy, is the preferred solution.

Various approaches using remotely sensed imaging spectroscopy data have been developed for mapping traits of terrestrial vegetation at different spatial scales (Ač et al., 2009; Asner et al., 2016, 2017; Malenovský et al., 2013; Pottier et al., 2014; Skidmore et al., 2015). Since optical remote sensing can be conducted from several platforms simultaneously (ground, towers, drones, aircraft and satellites), it provides the potential to merge information acquired at different spatial scales (from leaves, shoots, branches, crowns to canopies) with the temporal scale of dynamic ecosystem processes (e.g. plant photosynthetic and/or stress physiological reactions). This unique ability plays an essential role in multi-scale ecological observational networks, as for example within the National Ecological Observatory Network (NEON) (Kampe, Johnson, Kuester, & Keller, 2010). The spatio-temporal scaling capabilities of the three most frequently used remote sensing techniques, i.e. radiative transfer modelling, spectral un-mixing and multisensor data fusion, have been reviewed by Malenovský et al. (2007). Despite the rapid development in spectral digital imaging technology (both hardware and software), there will always be an

operational trade-off between the spatial/spectral and temporal resolutions of high-altitude airborne and satellite images. In particular, insufficient resolution and sampling frequencies create significant methodological limitations in monitoring the spatially extensive, but patchy and temporally dynamic, short-stature vegetation communities that dominate montane, tundra, polar, arid and semi-arid landscapes. Although space-borne mapping of these spatially fragmented vegetation types has intensified with the availability of multispectral satellite images of relatively high spatial resolution (c. 2 m) (Bricher, Lucieer, Shaw, Terauds, & Bergstrom, 2013; Liu & Treitz, 2016; Shin, Kim, Kim, & Hong, 2014), its operational use remains limited. For example, in the Antarctic operational obstacles include frequent cloud cover and instrument performance constraints, e.g. coarse spectral resolution and unacceptably long satellite revisit intervals (polar summers last just a few months).

Modern unmanned aircraft systems (UAS), also known as drones, can bridge the observational gap between detailed, but laborious and spatially limited field measurements and satellite images covering extensive areas at a relatively coarse resolution. In this study, we introduce a new non-invasive approach for measuring health in short-stature plant functional types, which scales ground-measured spectral signatures up to UAS spectral observations using a machine-learning method. The method is based on hyperspectral images of sub-decimeter spatial resolution, acquired with low-altitude imaging spectroscopy UAS (Aasen, Burkart, Bolten, & Bareth, 2015; Lucieer, Malenovský, Veness, & Wallace, 2014). We compare the ability of multispectral satellite and hyperspectral UAS image data with the highest achievable spatial resolution to map plant environmental stress indicators using the moss-dominated coastal ecosystems of East Antarctica as a model plant community.

## 2 | MATERIALS AND METHODS

### 2.1 | Study sites, species and plant characteristics

The study was conducted in the Windmill Islands of East Antarctica (Figure 1) at two pilot research sites: Antarctic Specially Protected Area 135 (ASPA; 66.282°S, 110.539°E) and Robinson Ridge (Robbos; 66.368°S, 110.586°E) (Clarke & Robinson, 2008; Robinson et al., 2005). The ice-free habitats of this region support some of the most extensive and best-developed moss-beds on Continental Antarctica. Summer melt water, in streams and melt lakes, sustains populations of three moss species including the Antarctic endemic moss *Schistidium antarctici* (Cardot) L.I. Savicz & Smirnova, and two cosmopolitan species, *Bryum pseudotriquetrum* (Hedw.) Gaertn., Meyer & Scherb. and *Ceratodon purpureus* (Hedw.) Brid.

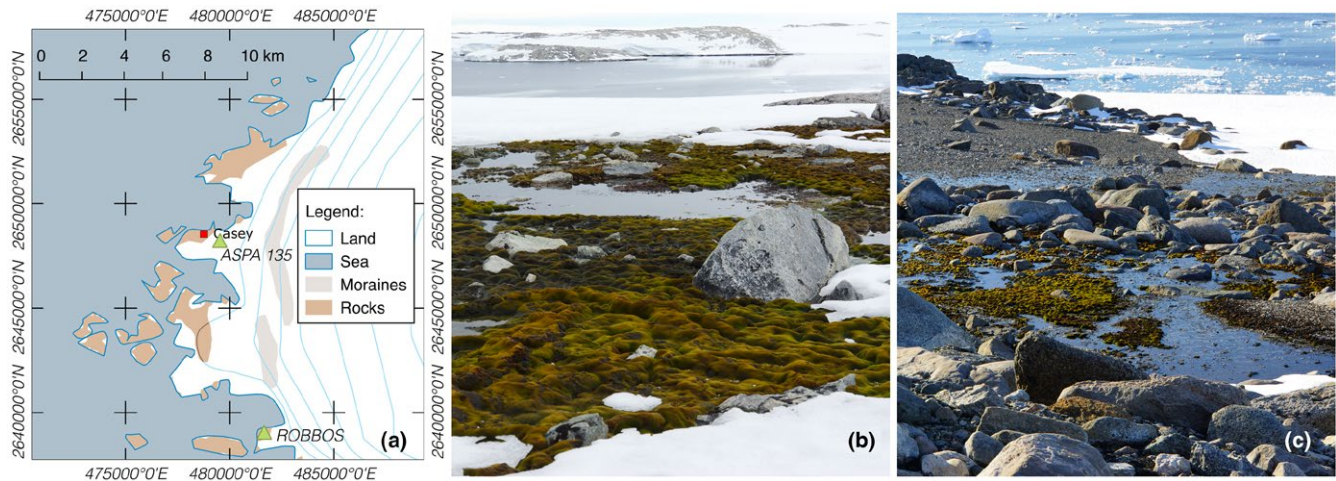


**FIGURE 1** Map of the Windmill Islands (a) of East Antarctica (UTM Zone 49 South, WGS84) with locations and photographs of moss beds at two research sites in the vicinity of Australian Casey station: (b) the Antarctic Specially Protected Area (ASP) 135 and (c) Robinson Ridge (Robbos)

These mosses are able to freeze and thaw, as well as desiccate and rehydrate, without losing chlorophyll pigments (Lovelock, Jackson, Melick, & Seppelt, 1995). Barring extreme stress, such as chronic photoinhibition, chlorophyll content is likely to change relatively slowly (days) in relation to environmental light exposure (Robinson et al., 2005) and other chronic environmental stresses enhanced from time to time by intensive acute disturbances. Effective leaf density (ELD), measured by counting the number of leaflets within a given length of gametophyte stem (Robinson et al., 2005), is a morphological and canopy structural stress indicator that responds to both growth form (changing within days) and hydration state (changing rapidly within minutes to hours). In the long-term, a range of environmental pressures may reduce stem elongation and increase leaf density (Clarke et al., 2012; Potters, Pasternak, Guisez, & Jansen, 2009; Waite & Sack, 2010). In the short-term, ELD can increase rapidly as a result of sudden reversible leaf shrinking and curling due to water loss (for more details see Malenovský, Turnbull, Lucieer, & Robinson, 2015).

## 2.2 | Remote sensing vegetation stress indicators

Physiological fitness of plants, including Antarctic mosses, can be empirically inferred from spectral vegetation indices (Jackson & Huete, 1991), which are mathematical transformations of remotely sensed light reflected by vegetation canopies (Myneni, Hall, Sellers, & Marshak, 1995). An example is the red edge inflection point (REIP), which represents the wavelength of the maximum slope of the prominent increase in vegetation reflectance between 680 and 750 nm (Horler, Dockray, Barber, & Barringer, 1983). Stress indication from vegetation indices is, however, often physiologically ambiguous. Although shifts in the REIP, from longer to shorter wavelengths, can indicate plant stress exposure, they can be caused by various factors: (1) geometrical changes in leaf angularity (plant wilting), (2) sudden declines in green chlorophyll pigments (foliage discolouration; Phoenix & Bjerke, 2016), (3) decreases in foliage biomass (leaf shedding) or (4) a

combination of these and other features (Vogelmann, Rock, & Moss, 1993).

To distinguish and separate the different types and causes of Antarctic moss stress reactions, we based our assessment on spectral retrievals of the two quantitative traits: (1) total chlorophyll *a* and *b* content (Cab; nanomoles of chlorophyll *a* and *b* molecules per gram dry weight) and (2) ELD (mean number of leaflets per millimetre of moss gametophyte). Declines in Cab indicate biochemical changes within the cell, while high ELD suggests slow growth and/or acute turf desiccation.

## 2.3 | Laboratory spectral experiments

Our nonintrusive remote sensing method expands upon a series of spectral drought-rehydration experiments conducted with small patches of Antarctic moss turf at Casey Station (66.283°S, 110.527°E) by Malenovský et al. (2015) in 2013 and spectral baseline measurements performed in 1999 by Lovelock and Robinson (2002). New imaging spectroscopy retrieval methods were successfully developed for remote sensing estimation of the two biophysical stress indicators, Cab and ELD, using support vector regression (SVR) algorithms (Smola & Schölkopf, 2004). Chlorophyll *a* and *b* content was estimated from moss canopy continuum-removed reflectance (i.e., reflectance normalized to a common baseline) of specific chlorophyll absorption wavelengths (648–715 nm) and ELD from reflectance of near infrared wavelengths (708–782 nm). A single indicator of moss relative vigour (RVI) was inferred by combining the retrieved estimates for Cab and ELD, which were scaled (0–1) and subsequently averaged. Malenovský et al. (2015) demonstrated that this approach is transferable from standardized laboratory spectral measurements to ground-based Antarctic moss hyperspectral images of matching wavelengths acquired at different field locations. This study scales the approach further to airborne (UAS) and WorldView-2 (WV2) satellite spectral imagery.

## 2.4 | WorldView-2 satellite image data

The 8-band multispectral WV2 images (DigitalGlobe, Inc., Westminster, CO, USA) of the Windmill Islands were acquired on 30 January 2011 for Robbos and 7 February 2011 for ASPA. Preceding data analysis, satellite images require specific processing that transforms the recorded signal from sensor units to units of radiance and corrects for confounding optical effects of atmospheric gases and aerosols, particularly their light scattering and absorption. Radiometric calibration, converting the 11-bit image of digital counts to physically meaningful radiance, was performed with WV2 calibration coefficients available in the ENVI/IDL image processing software (Harris Geospatial Solutions/Exelis Visual Information Solutions, Inc., Boulder, CO, USA). Atmospheric correction was carried out with the fast line-of-sight atmospheric analysis of hypercubes (FLAASH) module. A mid-winter latitude atmospheric scenario was selected with a visibility of 40 km. The water vapour column multiplier was derived from the Moderate Resolution Imaging Spectroradiometer (MODIS) water vapour products (MOS08\_D3), resulting in a water vapour column of 0.443 cm (30 January 2011) and 0.377 cm (7 February 2011). The required satellite sensor zenith and azimuth angles were derived from the WV2 metadata. The resulting reflectance images were projected into the Universal Transverse Mercator map coordinate system (UTM Zone 49 South, datum WGS84) at a pixel resolution of 2.2 m.

Moss health assessment was performed only for WV2 pixels with >50% abundance of vigorous moss. In the first step, pixels containing moss of any physiological state were identified by computing the normalized difference vegetation index (NDVI) (Tucker, 1979) from reflectance of red (630–690 nm) and first near infrared (770–895 nm) WV2 bands and selecting those with NDVI > 0.60. This step separated parts of images containing just abiotic material from those also containing some percentage of biotic material, i.e. moss canopy. In the second step, we filtered out pixels that contained predominantly bare soil with rocks and/or moss in an extremely stressed stage, designated as moribund (nearly dead), i.e. pixels with abundance of vigorous moss ≤50%. The spectrally pure reference signature of the vigorous moss was identified through calculating a minimum noise transformation and the pixel purity index from pixels selected in the first step. The spectral mixture tuned matched filtering (MTMF) technique was then applied to compute the relative similarity with the moss reference spectrum and to approximate the sub-pixel abundance of mosses. Finally, we identified pixels containing >50% of vigorous moss.

## 2.5 | Unmanned aircraft imaging spectroscopy data

The design and basic description of the unmanned aircraft imaging spectroscopy system (UAS) deployed in Antarctica are depicted in Figure 2. The UAS consisted of a micro-Hyperspec (Headwall Photonics, Inc., Fitchburg, MA, USA) visible and near infrared push-broom imaging spectrometer mounted to an Aeronavics Skyjib multirotor heavy-lift airframe. The micro-Hyperspec, equipped with an objective of 8 mm focal length, a field of view (FOV) of 49.8°, a slit

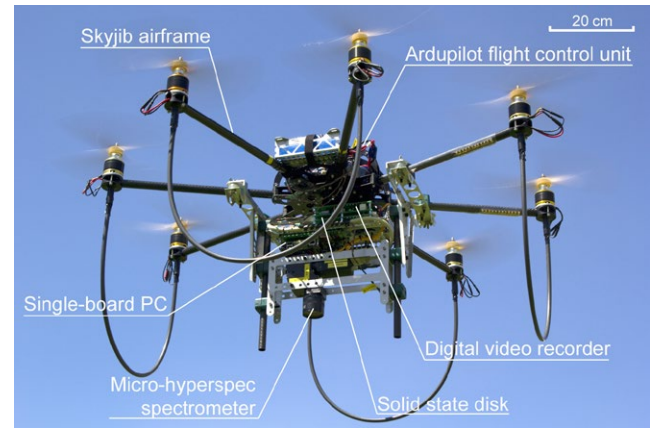


**FIGURE 2** Design of the hyperspectral unmanned aircraft system (HyperUAS) (Lucieer, Malenovsky, et al., 2014) with description indicating position of every essential system component

entrance of 25  $\mu\text{m}$  and a 12-bit charge-coupled device (CCD) of 1,004 pixels, was set in a binned mode with the frame period and integration time of 20 ms, resulting in a maximum rate of 50 frames/s. It was flown in stabilized mode 11 m above ground level at a constant speed of 2.5 m/s, while acquiring imagery of 162 spectral bands between 361 and 961 nm, with a bandwidth from 4.75 to 5.25 nm and a spatial resolution of 5.0 cm. The UAS was operated manually, as its autopilot instruments did not navigate reliably due to local deviations in Earth's magnetic field in polar regions (e.g.  $-100^\circ$  declination at Casey Station). Hyperspectral images of two, c. 30 m long and 10 m wide, transects were acquired at the ASPA site on 2 and 8 February 2013 (clear sky conditions). Two additional images were collected at Robbos on 5 and 6 February 2013 (full overcast conditions)—see Supporting Information Video S1.

Similar to satellite images, the raw hyperspectral data were radiometrically standardized and corrected for atmospheric interferences. Spectral values of reflected light recorded in 12-bit digital counts were converted to physical units of at-sensor radiance ( $\text{mW cm}^{-2} \text{sr}^{-1} \mu\text{m}^{-1}$ ) and to relative reflectance by applying sensor-specific radiometric calibration coefficients and an empirical line atmospheric correction as described in Lucieer, Malenovsky, et al. (2014)—see Supporting Information Video S2. Per-band radiometric calibration coefficients for the micro-Hyperspec sensor were obtained by measuring four known (pre-calibrated) spatially homogeneous light intensities produced in a certified optical integrating sphere USR-SR 2000S (Labsphere, Inc., North Sutton, NH, USA). Atmospheric correction coefficients were computed by coupling laboratory-measured reflectance of five spectral calibration panels (near-Lambertian flat reflectance responses ranging from 5% to 70%) with radiance values of the same panels recorded and extracted from UAS micro-Hyperspec images of both study sites.

The accuracy of the resulting UAS reflectance was verified against ground measurements of several spatially homogeneous natural targets. Reflectance of six large rocks and nine green moss patches was collected just after hyperspectral image acquisitions with an ASD HandHeld-2 spectroradiometer (ASD, Inc. & PANalytical, Boulder, CO,



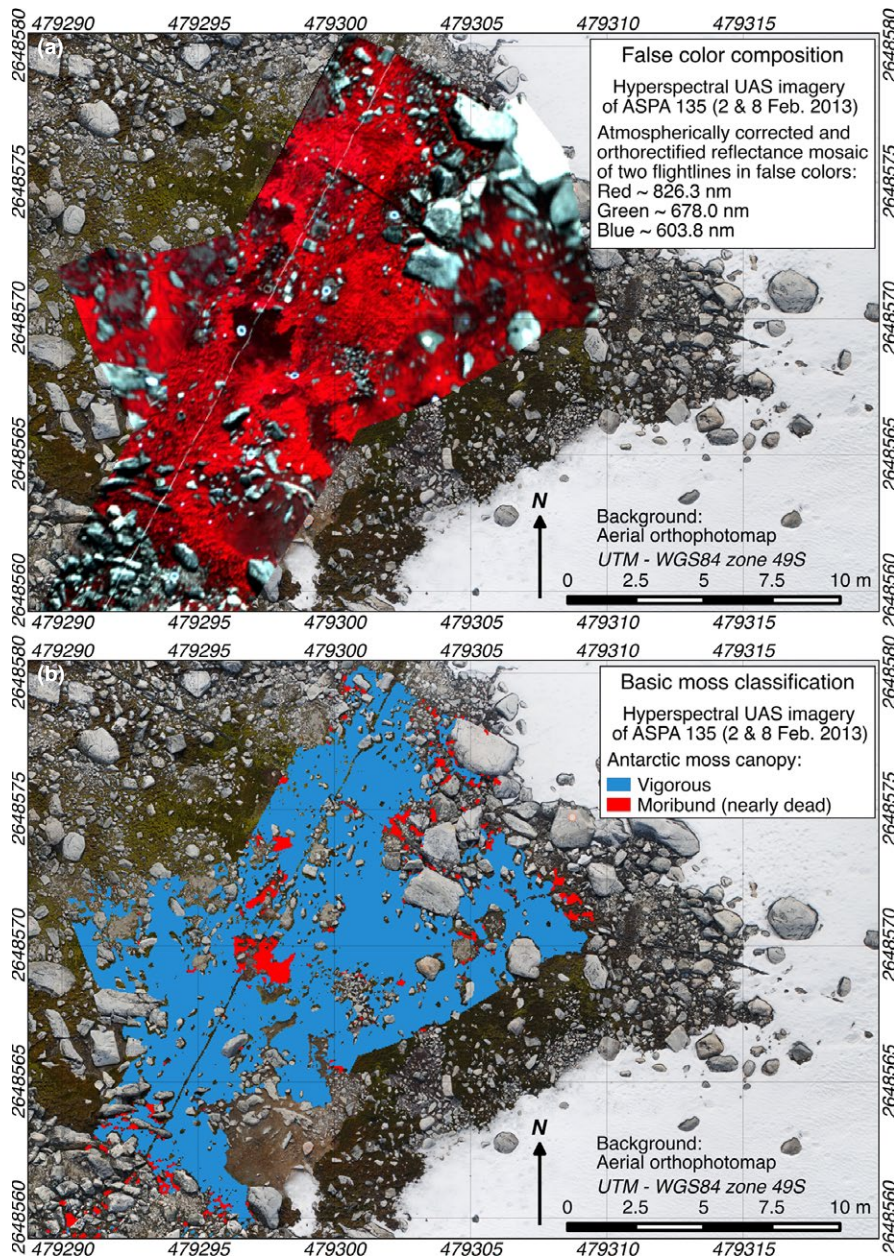


**FIGURE 3** False color composition of pre-processed unmanned aircraft system (UAS) hyperspectral mosaic (a) and basic classification of moss bed (b) located in Antarctic Specially Protected Area (ASPA) 135 (66.282°S, 110.539°E)

USA). Their reflectance signatures, extracted from remotely sensed UAS data, were found to be fully comparable with the independent ground-based measurements (see Supporting Information Data S1 and S2).

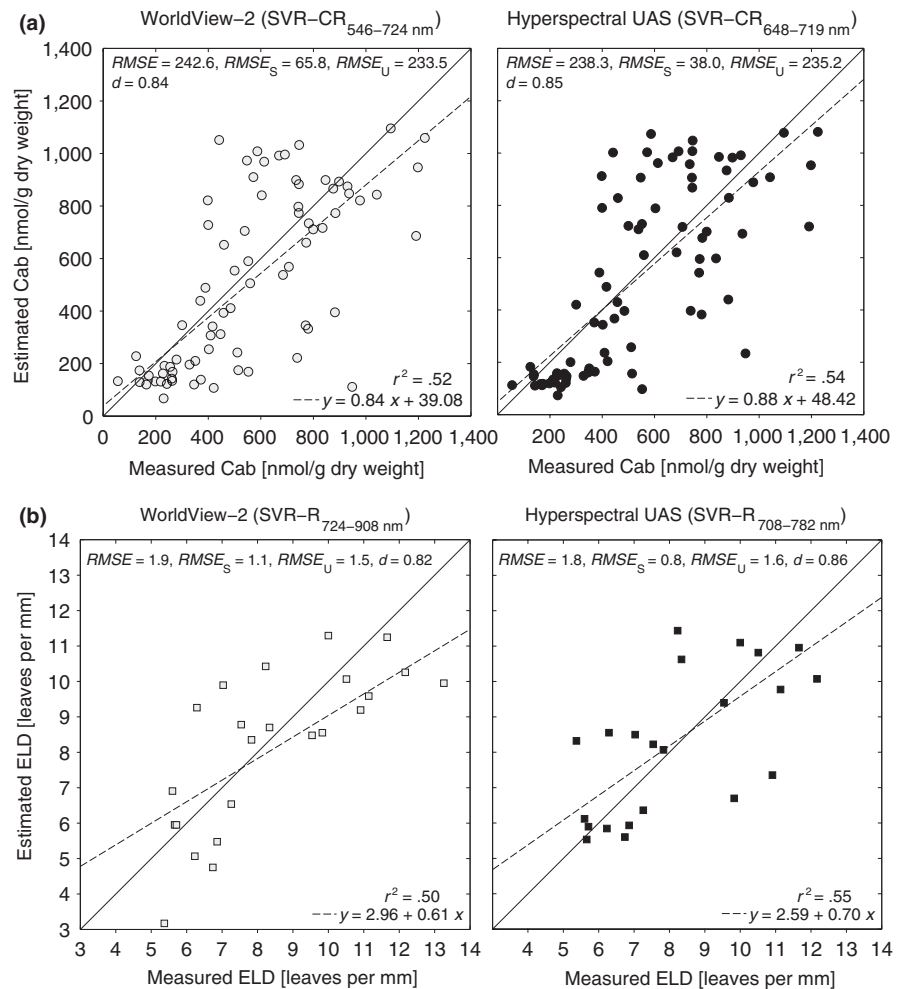
To facilitate production of geographically correct maps, the hyperspectral images were orthorectified with detailed (1 cm resolution) three-dimensional digital surface models that were derived from multiple overlapping UAS-collected orthophotographs (Lucieer, Turner, King, & Robinson, 2014). Each image was subsequently transformed into the map coordinate system of WGS84 UTM zone 49 South by a rubber sheeting triangulation using 50 evenly distributed artificial ground control points (aluminium discs). The control points were coordinated with survey-grade real-time kinematic global positioning system (GPS) receivers, achieving an absolute geometric accuracy of 2–4 cm. Geocoded flight lines were mosaicked per site in a single airborne image (Figure 3a).

The high spatial resolution of the UAS mosaics (5 cm) allowed detection of spectrally pure pixels containing only moss turf. Narrow bands at 670.55 and 800.34 nm were transformed to NDVI, and non-vegetated pixels with  $NDVI < 0.75$  were masked out. A threshold of a modified triangular vegetation index 2 (Haboudane, Miller, Pattey, Zarco-Tejada, & Strachan, 2004)  $MTVI2 \geq 0.25$  enabled us to distinguish pixels containing moribund moss from pixels of vigorous moss canopy (Figure 3b). Only the latter class was used in SVR-based estimation of stress indicators and health assessment.

## 2.6 | Support vector regressions

The application of machine learning in remote sensing and geosciences in general has grown rapidly in recent years (Lary, Alavi, Gandomi, & Walker, 2016). These modern techniques have several

**FIGURE 4** Validation of support vector regressions (SVR) estimating (a) chlorophyll *a* + *b* content (Cab) and (b) effective leaf density (ELD) of Antarctic mosses from reflectance measurements convolved to spectral bands of satellite WorldView-2 and unmanned aircraft system (UAS). Cab estimates ( $n = 80$ ) were retrieved with SVR from continuum-removed (CR) reflectance of chlorophyll absorption wavelengths (SVR-CR<sub>546–724 nm</sub> and SVR-CR<sub>648–719 nm</sub>), whereas SVR trained with reflectance (*R*) intensities of near infrared wavelengths (SVR-R<sub>724–908 nm</sub> and SVR-R<sub>708–782 nm</sub>) were used to predict ELD ( $n = 24$ ). Solid line indicates the expected one-to-one linear relationship and dashed line is the linear regression function computed between analytically measured and SVR estimated values. RMSE, root-mean-square error; RMSE<sub>S</sub>, systematic components of RMSE; RMSE<sub>U</sub>, unsystematic components of RMSE; *d*, index of agreement;  $r^2$ , coefficient of determination



advantages, when compared to traditional statistical approaches (e.g. regressions), they: (1) cope well with large high-dimensional datasets of non-normally distributed variables, (2) are robust to model overfitting, and (3) can generalize a prediction problem even with limited training samples. Additionally, they also have an in-built mechanism for quantifying model fit and input variable importance (Üstün, Melssen, & Buydens, 2007). Random forest (Belgiu & Drăguț, 2016) and support vector machines (Mountrakis, Im, & Ogole, 2011) were applied to classify land cover types, but also to estimate quantitative parameters of vegetation from remotely sensed images (Verrelst et al., 2015). We used the epsilon-SVR training optimization technique with the nonlinear Gaussian radial basis function (RBF) kernel to estimate Cab and ELD as described in Malenovsky et al. (2015). The laboratory reflectance measurements of moss canopies, acquired in 2013 and 1999 with a sampling interval of 1 nm, were first convolved in bandwidths and spectral sampling intervals of WV2 and micro-Hyperspec sensors in accordance with their specific spectral response functions. After this preprocessing, they were coupled with corresponding Cab and ELD values and scaled by assigning the mean of each dataset to zero and its standard deviation to one. The epsilon-SVR, available in the C++ library for support vector machines known as LIBSVM, was presented with the moss spectral characteristics as inputs and their related biochemical/physical traits

as outputs. A dual optimization grid-search, combined with a five-fold cross-validation that prevents overfitting of a trained model, was applied to find the best-performing prediction models with the minimum mean square error (MSE) between estimated and provided outputs.

The optimization identified four continuum-removed WV2 reflectance bands located between 546 and 724 nm and 20 UAS bands positioned between 648 and 719 nm, respectively, as the most suitable SVR inputs to predict Cab. Three WV2 reflectance bands from 724 to 908 nm and 21 UAS bands from 708 to 782 nm, respectively, were found to be the most optimal for estimation of ELD. Cab predicting SVR algorithms were trained with WV2 and/or UAS convolved laboratory measurements collected in 2013 ( $n = 54$ ) and validated with measurements from 1999 ( $n = 49$ ). Since leaf density of moss samples was measured only in 1999, the dataset was split into 2/3 training ( $n = 49$ ) and 1/3 testing samples ( $n = 24$ ), while maintaining the Gaussian distributions of leaf densities in both subsets. Once properly trained, the models were executed in a prediction mode. Although the best performing WV2 and UAS regressions used less spectral inputs of different bandwidths, they produced Cab and ELD estimates of similar accuracies (Figure 4). This is attributed to high spectral purity and good signal-to-noise ratio of moss reflectance measured in the laboratory.



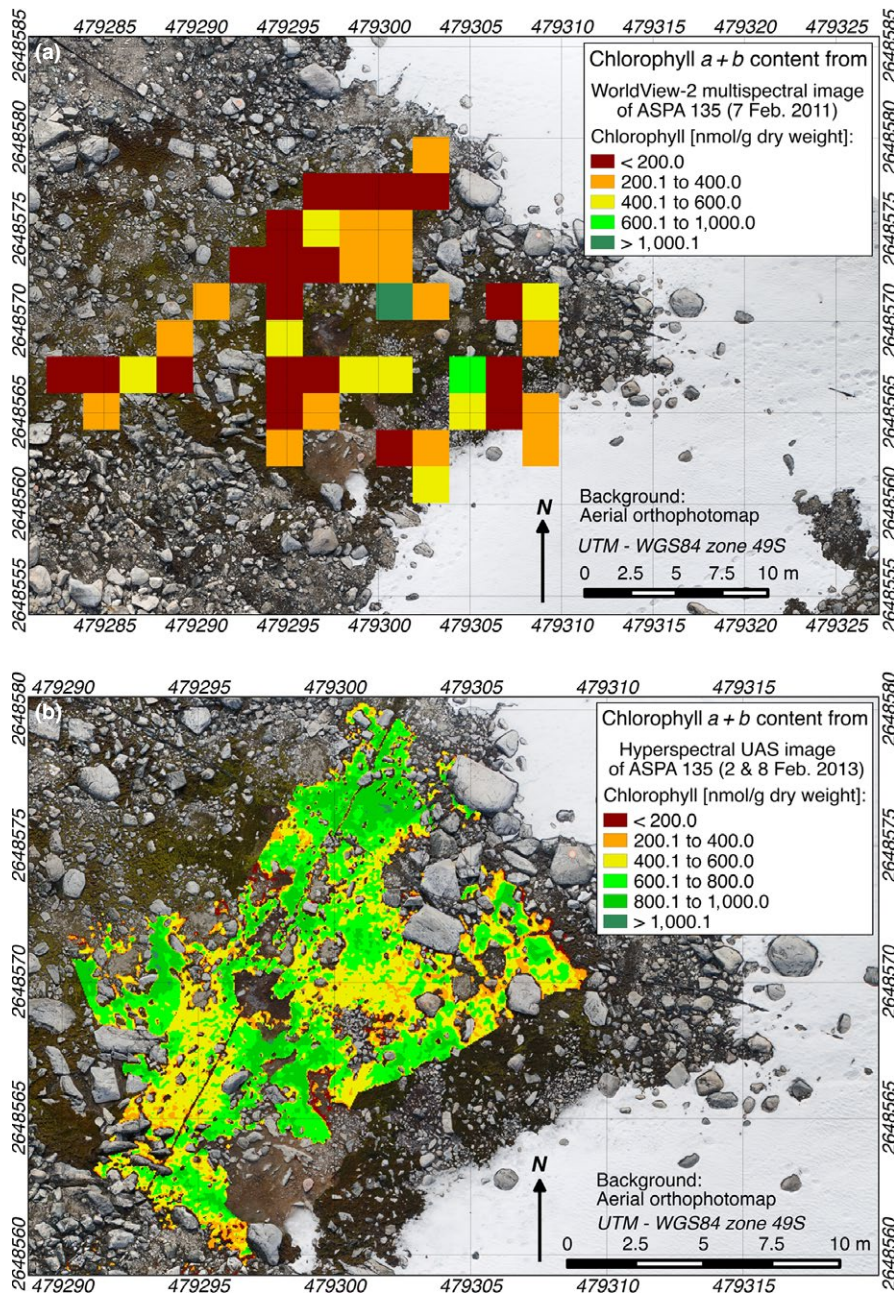


**FIGURE 5** Chlorophyll *a + b* content of vigorous mosses estimated by (a) SVR-CR<sub>546–724 nm</sub> from WorldView-2 and (b) SVR-CR<sub>648–719 nm</sub> from hyperspectral unmanned aircraft system data (for more details see Figure 4) for Antarctic Specially Protected Area (ASP) 135 research site

The best-performing SVR models were applied per pixel on vigorous moss canopies identified in WV2 and hyperspectral UAS images. Cab and ELD per-pixel estimates (Figures 5 and 6) were scaled between zero and their largest value obtained in the laboratory (i.e. Cab of 1,500 nmol/gdw and ELD of 15 leaves per mm). Scaled values of Cab and inverted ELD were averaged to assess the relative moss vigour (RVI), where RVI = 100% indicates optimally growing healthy moss, whereas RVI = 0% reveals moss highly stressed by unfavourable conditions.

## 2.7 | Ground-based verification of remote sensing indicators

Verification of remotely sensed moss health indicators was performed with data from a long-term monitoring project of Windmill Islands'

plant communities. We utilized several permanent quadrat locations, which were established at ASPA and Robbos study sites in 2003 (Australian Antarctic Data Centre, 2009; Wasley et al., 2012). Digital red-green-blue (RGB) composite photographs of these quadrats, taken between 16 and 27 January 2013 with a Sony DSC-HX9V camera (Sony Corp., Tokyo, Japan), were processed in a semi-automatic way, which reduced time requirements and subjectivity of manual processing and ensured consistency of image interpretation. The photographs were imported into the ArcGIS geographical information system (ESRI, Redlands, CA, USA), spatially scaled to the real quadrat size (25 × 25 cm<sup>2</sup>) and georeferenced to their corresponding GPS locations. Polygons defining physical borders and masking out large rocks were digitized over each quadrat. The pre-processed images and masks were imported into the eCognition software (Definiens



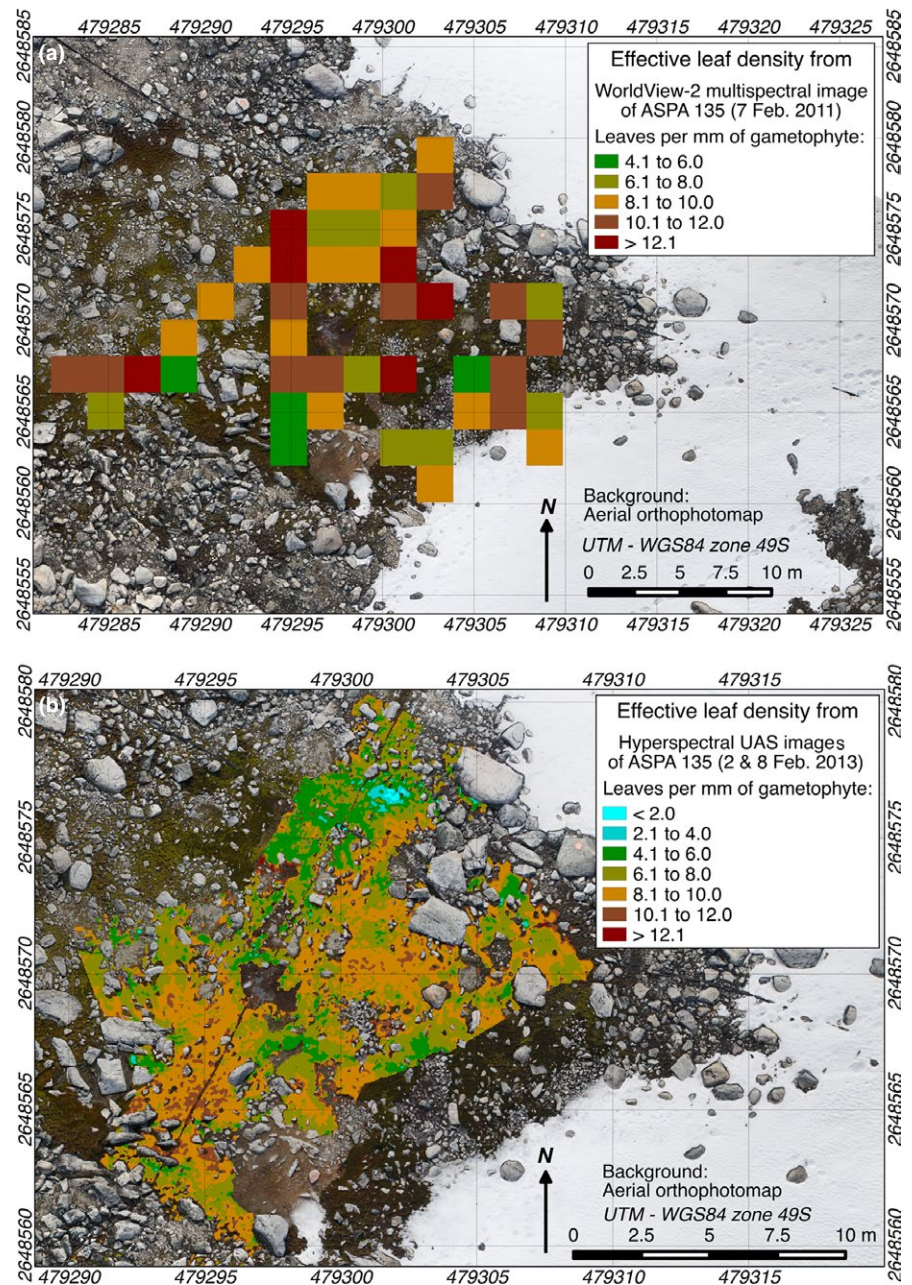


**FIGURE 6** Effective leaf density of vigorous mosses estimated by (a) SVR- $R_{724-908\text{ nm}}$  from WorldView-2 and (b) SVR- $R_{708-782\text{ nm}}$  from hyperspectral unmanned aircraft system data (for more details see Figure 4) for Antarctic Specially Protected Area (ASPA) 135 research site

Imaging GmbH, München, Germany) for object-based image analysis (OBIA) and semi-automatic classification. Optimal settings for multi-resolution image object segmentation were determined using the estimation of scale parameter (ESP) tool (Drăguț, Tiede, & Levick, 2010). Image segmentation was performed using a scale parameter of 33, with parameters of colour/shape set at 0.9/0.1 and smoothness/compactness at 0.5/0.5. The subsequent OBIA image classification, which used a set of rules related to RGB band digital value thresholds, was applied to separate vegetation within the quadrats into healthy, stressed and moribund moss, in addition to a class of residual stones. Results of the OBIA classification of selected images were compared with outputs of a visual classification, resulting in an overall accuracy of 84%. The relative cover (%) of healthy, stressed and moribund moss, as quantified in 13 quadrats located in hyperspectral imagery,

was compared to the UAS-based moss vigour indicators to verify their validity. Validation of WV2 results was not performed due to incomparable scales (satellite pixel size of  $4.84\text{ m}^2$  vs. size of field monitoring quadrats of  $0.0625\text{ m}^2$ ) and the 23-month gap between the WV2 image and field data collections.

## 2.8 | Statistical analyses

Several tests were employed to assess the statistical significance of our results. Boxplot diagrams, with the centre point representing the median of compared datasets, were constructed to demonstrate statistical differences between estimates from WV2 and UAS data. If the notches of two boxplots do not overlap, one can conclude with 95% confidence that their true medians differ. Interval endpoints are the



extremes of the notches that correspond to  $q_2 - 1.57(q_3 - q_1)/\sqrt{n}$  and  $q_2 + 1.57(q_3 - q_1)/\sqrt{n}$ , where  $q_2$  is the 50th percentile (median),  $q_1$  and  $q_3$  are the 25th and 75th percentiles, respectively, and  $n$  is the number of observations. Points were drawn as outliers (open circles), if they were larger than  $q_3 + w(q_3 - q_1)$  or smaller than  $q_1 - w(q_3 - q_1)$ , where the length of whiskers  $w = 1.5$  covered c. 99.3% of normally distributed data.

Anticipated relationships between remotely sensed and ground measured variables were tested via linear regressions and by computing comparative statistical indicators. The coefficient of determination ( $r^2$ ) was used to assess how much of the variability in ground truth derived from quadrat photographs (acting as independent variables) could be explained by regressed spectral estimates of health (acting as dependent variables). The Student's  $t$  test was applied to calculate probability ( $p_{t \text{ test}}$ ) of the linear regression slope being equal to zero. Root mean square error (RMSE), including its systematic ( $RMSE_S$ ) and unsystematic ( $RMSE_U$ ) components, and a dimensionless index of agreement ( $d$ ) provided more detailed assessment of retrieval accuracies (Willmott, 1981). If  $RMSE_S > RMSE_U$ , then the retrieval errors originate from the predictive SVR model and such models will always yield systematically biased estimates. In the opposite situation ( $RMSE_S < RMSE_U$ ), the model is as good as it can be and the retrieval bias is caused by random errors originating from measurement inaccuracies and noise contamination. According to Willmott (1981), the index of agreement indicates the degree to which the observed deviations of the mean measurements correspond in magnitude and sign to the predicted deviations of mean estimations. Full agreement between estimates and observations is denoted by  $d = 1.0$ , whereas  $d = 0.0$  signals their complete disagreement.

### 3 | RESULTS

#### 3.1 | Remotely sensed indicators of antarctic moss health

The Cab and ELD estimates from moss reflectance acquired during indoor experiments at Casey station and convolved to WV2 data were fully comparable with results of the laboratory measurements converted into narrow hyperspectral UAS bands (Table 1). This is despite the fact that SVR routines trained for WV2 data used fewer spectral bands of considerably wider bandwidths. Although  $RMSE_S$  were found to be slightly higher for WV2, they were significantly lower than the corresponding  $RMSE_U$  for both WV2 and UAS results. This indicates that prediction errors are primarily caused by random noise in the model training and validation datasets, while the design of the predictive models is optimal and does not need any further improvements. Almost identical errors (RMSE of 242.6 and 238.3 nmol/gdw, and 1.9 and 1.8 leaves per mm for WV2 and UAS, respectively) suggest that SVR algorithms can use just 3–4 input spectral bands of appropriate wavelengths to estimate Cab and ELD with the best achievable accuracy, but only if trained with and applied to spectrally clean (100% pure) moss reflectance, as is the case for laboratory measurements.

**TABLE 1** Validation of support vector regressions trained for estimation of moss chlorophyll content and effective leaf density from spectral remote sensing data using laboratory measurements

Validation indicator <sup>a</sup>	Chlorophyll content		Effective leaf density	
	WV2	UAS	WV2	UAS
	[relative]		[relative]	
$r^2$	.52	.54	.50	.55
$d$	0.84	0.85	0.82	0.86
	[nmol/g dw]		[leaves per mm]	
RMSE	242.6	238.3	1.9	1.8
$RMSE_S$	65.8	38.0	1.1	0.8
$RMSE_U$	233.5	235.2	1.5	1.6

<sup>a</sup>The performance of support vector regressions in estimating moss traits from spectrally clean multispectral satellite WorldView-2 (WV2) and hyperspectral unmanned aircraft system (UAS) data was evaluated by: coefficient of determination ( $r^2$ ) of expected linear regression between estimates and measurements, index of agreement ( $d = 1.0$  indicates perfect agreement,  $d = 0.0$  complete disagreement), and root mean square error (RMSE) with its systematic ( $RMSE_S$ ) and unsystematic ( $RMSE_U$ ) components (for detailed information see Willmott, 1981).

Multispectral WV2 and hyperspectral UAS images were acquired at two research sites, ASPA 135 and Robbos, in February 2011 and 2013, respectively. The best-performing SVR algorithms were applied to multispectral WV2 pixels containing greater than 50% and hyperspectral UAS pixels containing 100% of vigorous moss canopies. Interpretation of local RVI maps (Figure 7) for the ASPA research site illustrates clearly the inadequate spatial resolution of WV2 satellite images. The map originating from UAS imagery (Figure 7b) shows a continuous pattern of RVI with a coherent contextual progression of high values (>50%) following the locally observed water drainage streams (Figure 7c). In contrast, the pattern obtained from WV2 data (Figure 7a) is scattered and discontinuous, with the equivalent water drainage locations exhibiting low RVI (<40%). This disparity is caused by confounding objects inside the 4.84 m<sup>2</sup> large WV2 pixels, particularly moribund moss, small pools, rocks, stones and bare soil, causing contamination of the vigorous moss-dominated spectral signal. The much smaller pixels of the UAS imagery (0.0025 m<sup>2</sup>) allow spatial delineation and removal of these objects.

Although ELD estimates obtained from WV2 and UAS data are similar (Figure 8b), the means of WV2 Cab values are more than 1.7 times lower than UAS estimates (Figure 8a), triggering systematic underestimation in WV2 vigour assessments (Figure 8c). The box-plots illustrate that ELD distributions are comparable (ELD medians: WV2 ~9.5 and 10.0 vs. UAS ~8.4 and 8.2 leaves per mm), whereas WV2 distributions of Cab estimates are shifted towards lower values (Cab medians: WV2 ~295.1 and 278.4 vs. UAS ~545.3 and 502.1 nmol/gdw). The WV2 RVI values are almost half the UAS ones (RVI medians: WV2 ~28.0 and 25.0 vs. UAS ~40.2 and 40.2%), due to the coarse WV2 spatial resolution causing spectral contamination of the moss chlorophyll absorption signal (650–720 nm) by higher reflectance of surrounding abiotic surfaces and moribund mosses.

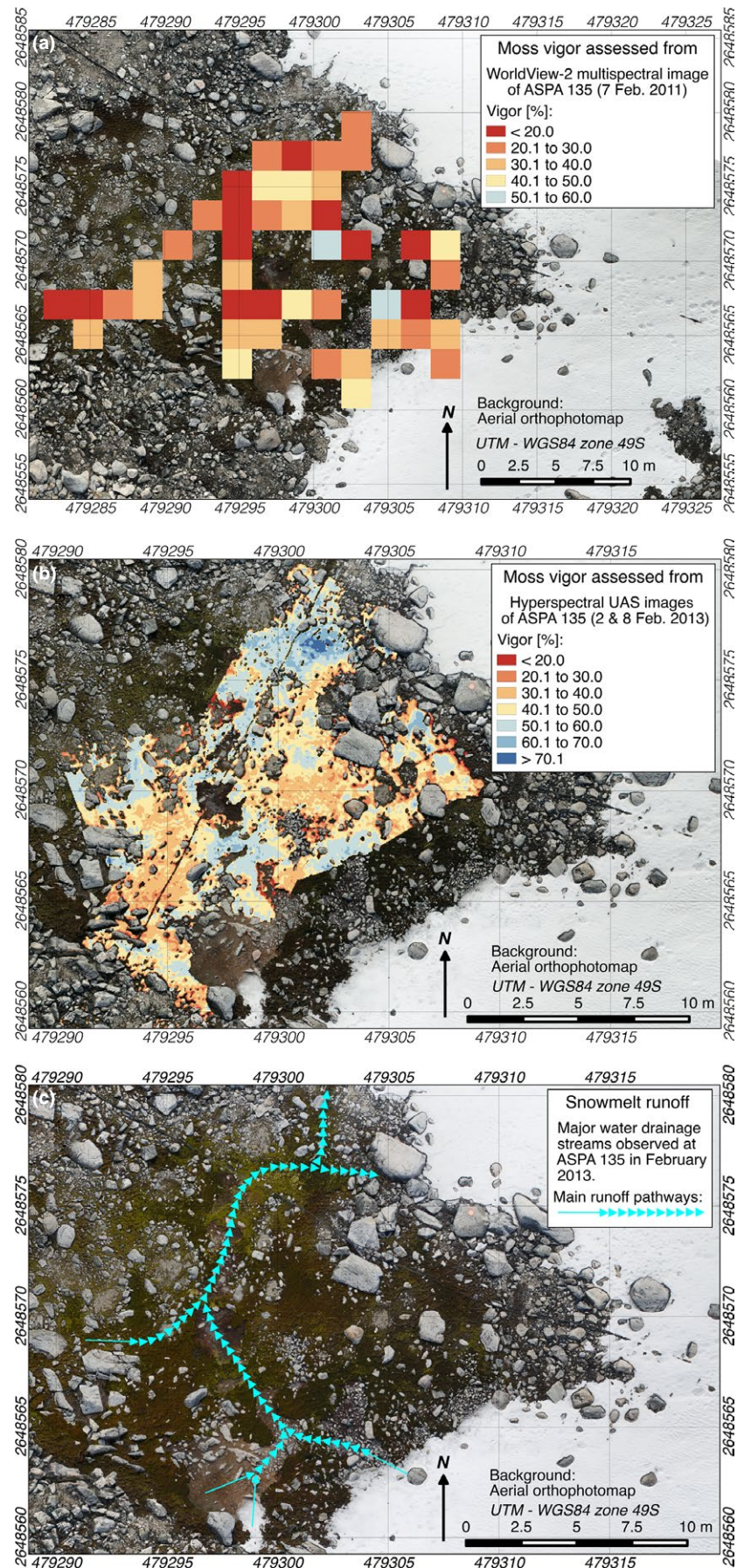


**FIGURE 7** Maps of relative moss vigour at the Antarctic Specially Protected Area (ASPA) 135 study site derived from (a) WorldView-2 multispectral image acquired on 7 February 2011 (pixels size 4.84 m<sup>2</sup>) and from (b) UAS hyperspectral image mosaic acquired on 2 and 8 February 2013 (pixel size 0.0025 m<sup>2</sup>). Map of snowmelt runoff (c) illustrates main water drainage pathways and runoff directions observed at ASPA 135 in February 2013



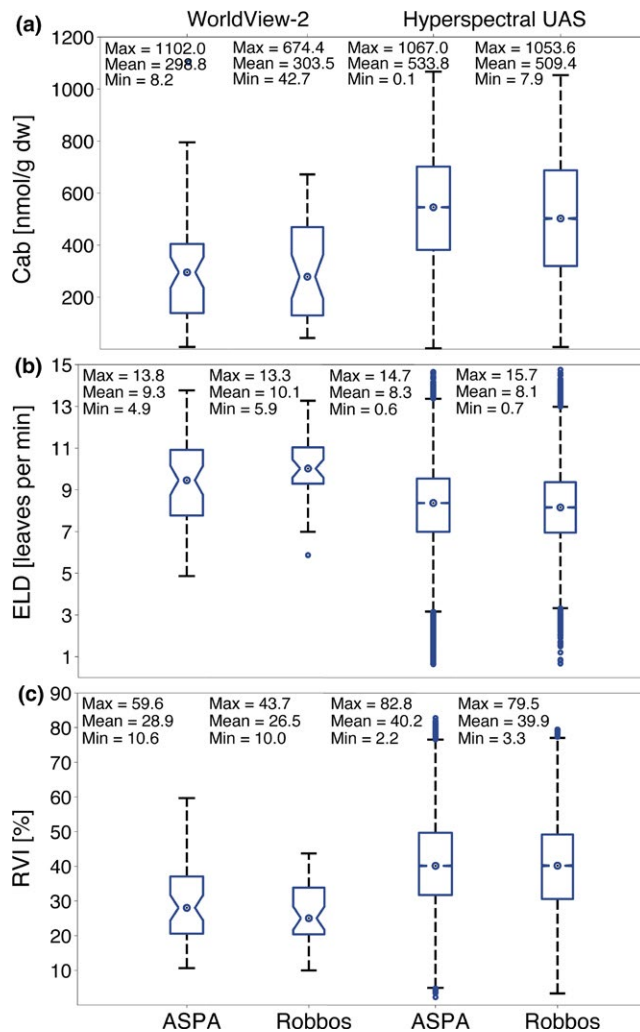


**FIGURE 8** Antarctic moss stress indicators derived from satellite WorldView-2 and unmanned aircraft system (UAS) spectral images. Boxplots display medians and 25th and 75th percentiles of (a) moss chlorophyll *a* + *b* content (Cab), (b) effective leaf density (ELD), and (c) relative vigour indicator (RVI). Moss traits were estimated from WorldView-2 pixels containing >50% of vigorous mosses (Antarctic Specially Protected Area [ASPA]: *n* = 50; Robinson Ridge [Robbos]: *n* = 40) and from UAS pixels of spectrally pure vigorous mosses (ASPA: *n* = 66,271; Robbos: *n* = 37,719). Dashed whiskers indicate 99.3% of normally distributed data and open circles represent estimates outside this range

### 3.2 | Correspondence of UAS maps with ground observations

The reliability of UAS maps was assessed using the 13 photographs of long-term monitoring vegetation quadrats, taken in January 2013, which were captured and located on hyperspectral flight lines. Relative abundance of healthy, stressed and moribund moss (Figure 9) was plotted against quantitative health indicators obtained at the same locations from UAS flights about 2 weeks later. The most significant positive linear relationship was obtained between relative amounts of healthy moss and mean RVI ( $r^2 = .71$ ,  $p_{t\text{ test}} < .0003$ ), followed by mean Cab ( $r^2 = .64$ ,  $p_{t\text{ test}} < .0010$ ; Figure 9a). Since increased stress

is associated with decreasing RVI and Cab values, significant negative relationships were revealed between relative abundance of moribund and/or stressed moss and mean RVI and/or Cab estimates ( $r^2 = .54$ ,  $p_{t\text{ test}} < .0040$  and  $r^2 = .60$ ,  $p_{t\text{ test}} < .0020$ ; Figure 9c, and  $r^2 = .50$ ,  $p_{t\text{ test}} < .0072$  and  $r^2 = .41$ ,  $p_{t\text{ test}} < .0185$ ; Figure 9b, respectively). Although weaker regressions were found for mean ELD predictions (healthy moss:  $r^2 = .46$ ,  $p_{t\text{ test}} < .0105$ , stressed:  $r^2 = .39$ ,  $p_{t\text{ test}} < .0226$ , and moribund:  $r^2 = .24$ ,  $p_{t\text{ test}} < .0921$ ), the combination of Cab and ELD in RVI resulted in highly significant relationships, which support the UAS-derived RVI map as a reliable measure of actual moss health.

## 4 | DISCUSSION

### 4.1 | Advantages and difficulties of spectral UAS monitoring

This study demonstrates that remote sensing imaging spectroscopy can assess stress in small-stature vegetation with comparable performance and greater efficiency than traditional ground techniques. Physical laboratory and field measurements, however, are and will remain essential for calibration and validation of such remote sensing methods. Spectrally mixed reflectance of WV2 satellite pixels containing less than 50% of spatially and temporally varying abiotic surfaces (e.g. rocks of different mineral compositions) caused underestimation of chlorophyll content. The relatively large and spectrally heterogeneous contribution of rock surfaces to the reflectance of WV2 pixels obscures subtle differences and changes in moss spectral signatures. The subsequent decrease in moss vigour could be incorrectly interpreted as indicating a decline in moss ecosystem health. Our new approach, using UAS hyperspectral images with a spatial resolution guaranteeing spectrally clean reflectance of any moss turf larger than 0.01 m<sup>2</sup>, delivered unbiased stress assessment. This superior performance of UAS is, however, not due to the higher number of spectral bands with narrower bandwidths, but in this case results from its more detailed spatial resolution, which matches the size of the spatially fragmented moss patches. The results presented in Figure 4 demonstrate that any spectrometer with about 4–6 suitably defined spectral bands should be able to accurately retrieve these moss traits. Therefore, a smaller, lighter and cheaper multispectral device could be sufficient for assessing the health of short stature vegetation communities in a quantitative manner. Nevertheless, this theoretical potential must be further investigated and practically tested before being recommended as a suitable UAS monitoring practice.

Space-borne maps derived from passive optical instruments are usually distributed as temporal composites of several satellite overpasses from consecutive days or even weeks. The temporal integration removes obscuring effects of clouds and their shadows, but this approach also reduces the temporal resolution of satellite maps and hence limits our ability to quickly identify sudden tipping points of ecosystems under stress. Unlike satellite sensors, UAS platforms can fly on demand and even collect data below clouds during overcast conditions. The signal-to-noise ratio of the micro-Hyperspec UAS spectrometer used in this study was sufficient to perform moss

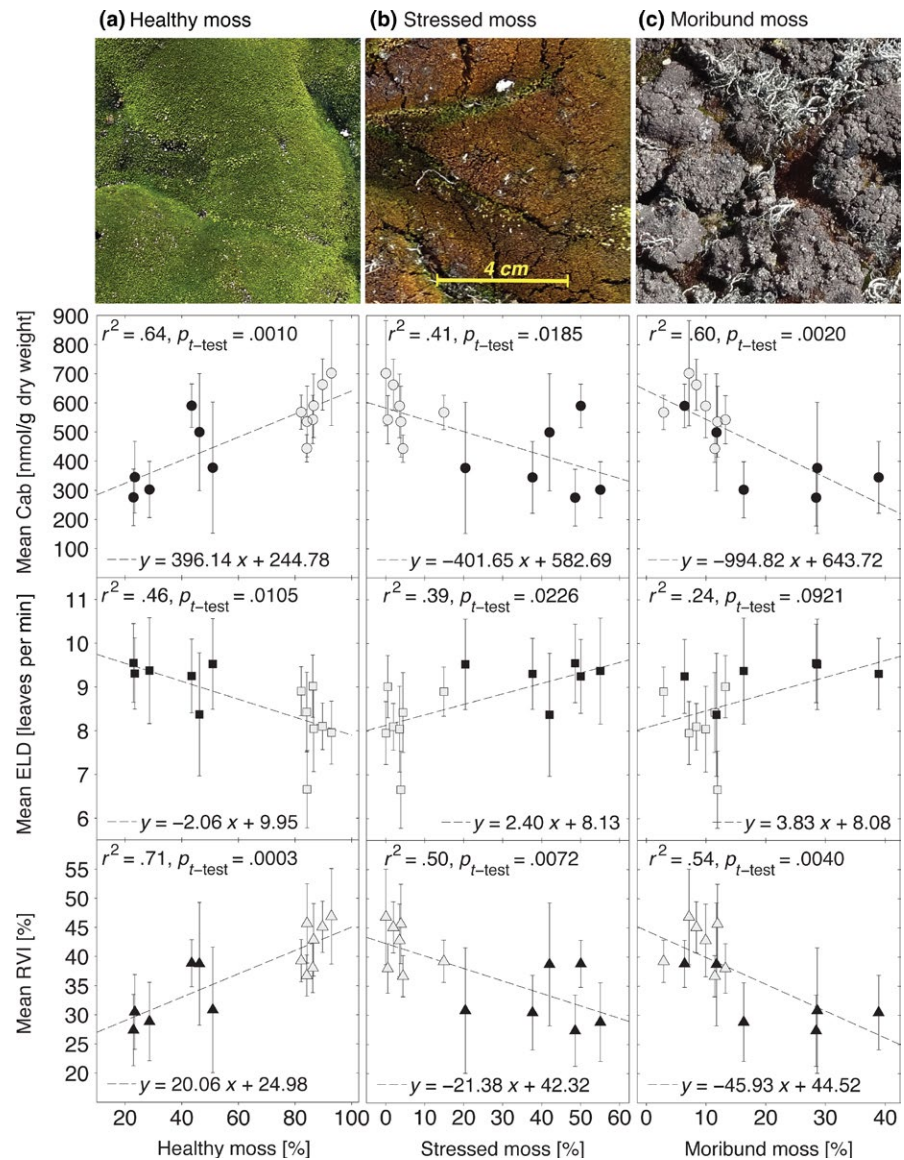


**FIGURE 9** Validation of stress indicators retrieved from hyperspectral UAS images. Linear regressions (dashed lines) were established between estimated chlorophyll *a* + *b* content (Cab), effective leaf density (ELD) and relative vigour indicator (RVI) and percentage of (a) healthy, (b) stressed, and (c) moribund (nearly dead) moss abundance observed in 13 permanent monitoring plots (size of 0.0625 m<sup>2</sup>) at Antarctic Specially Protected Area 135 (open symbols, *n* = 7) and Robinson Ridge site (closed symbols, *n* = 6). Stress indicators are given as mean ± standard deviation (*n* ranges from 25 (minimum) to 39 (maximum) hyperspectral image pixels) with coefficients of determination (*r*<sup>2</sup>) and probability of regression slope being equal to zero (*p*<sub>*t*-test</sub>)

assessment even under full cloud conditions (indirect diffuse irradiation; see Supporting Information Video S1), which prevail over clear-sky days in the coastal parts of East Antarctica. Under the assumption that spectrometers of comparable spectral quality will be used, UAS platforms might present the only solution for efficient remote sensing of vegetation in locations with frequent cloud cover, such as in the sub- and maritime Antarctic and Arctic.

On the other hand, there are also technical difficulties involved in operating UAS in Antarctica. The UAS electronic components are usually not designed for the cold temperatures, particularly the performance and endurance of the batteries. Unexpected wind gusts often impact upon the predefined flight trajectory of the UAS, which can introduce geometric distortions of images acquired with an airborne spectral scanner. Very strong wind gusts can potentially be destructive for small-size UAS airframes. Finally, our UAS autopilots, which rely on GPS technology combined with a magnetometer, were unable to operate under automatic navigation, most likely due to the local magnetic declination of 100° West. Consequently, all UAS missions were

operated manually within the line of sight over a relatively small study area. Nonetheless, we recently integrated the micro-Hyperspec push-broom scanner with associated positioning and orientation sensors on a new multi-rotor UAS airframe (DJI Matrice 600) and tested the platform's ability to auto-navigated along pre-defined flight lines. Also the most recent flight controllers repeatedly worked well when deployed in polar regions. We are, therefore, confident that with future UAS image acquisitions in Antarctica we are capable covering much larger areas based on auto-navigated flights.

## 4.2 | UAS for ecological applications: benefits and challenges

The field of ecological mapping with UAS platforms is rapidly developing, driven by the availability of smaller, lighter sensors with improved performance. The potential use of UAS technology in spatial ecology applications has been reviewed in Anderson and Gaston (2013). In general, the key benefit of UAS remote sensing is the ability to collect



ultra-high spatial resolution imagery (pixel size <10 cm), at required times and with multiple sensors covering a wide range of the electromagnetic spectrum. Such datasets can be collected at a relatively low cost compared to deployment of a manned aircraft or acquisition of a very high resolution commercial satellite image. The main power of UAS in ecological sampling is their ability to bridge the existing scale gap between detailed field observations (usually collected at small plots or along transects) and regional-to-global satellite observations. UAS allow us to study patterns and processes at centimeter scales over spatial extents of several hectares up to several square kilometers. This capability makes them an ideal tool for validation and perhaps also calibration of air-/space borne sensors, their acquisitions and products.

Colomina and Molina (2014), Cracknell (2017) and Pajares (2015) provide extensive reviews on state-of-the-art UAS technology and regulations in the context of remote sensing studies. Despite the noticeable benefits, a range of challenges needs to be resolved before conducting UAS acquisition of scientific data. First, any safe UAS operation needs piloting expertise and certification. In many countries, pilots are required to be legally certified for UAS operations through a piloting course concluded by theoretical and practical tests. Depending on local laws, UAS pilots have to keep the aircraft within visible line of sight, below 400 ft (120 m), and under effective control at all times. In addition, weather and environmental conditions such as strong winds (e.g. >25 knot gusts), shadow-casting patchy cloud cover, or the presence of protected wildlife (Hodgson & Koh, 2016) can impose limitations on the ability of UAS to collect data or to cover study areas of the required size. Despite the technological advances enabling UAS platforms to fly for longer (e.g. 30–60 min), the limitation of keeping a UAS within visual line of sight results in a maximum area that can be covered within a single flight of between 0.1 and 2 km<sup>2</sup>. The achievable spatial extent also depends on the size and type of aircraft used, with fixed-wing UAS generally able to cover larger areas than multi-rotor helicopters. Further advances in technology and safety features will likely foster relaxation of some rules. For example, a sub-2 kg weight class, introduced in Australia, USA, Canada and several European countries, has allowed relatively easy and flexible operations of small, light aircraft (Cunliffe, Anderson, DeBell, & Duffy, 2017). Considering recent advances in 3D mapping technology and miniaturization of optical cameras, these lightweight UAS are becoming highly efficient and powerful remote sensing data collection tools.

### 4.3 | Potentials in method advancements

Although our remote sensing technique was developed for monitoring moss communities in East Antarctica, it is also applicable to other small-stature vegetation communities. However, further laboratory and/or field studies would be needed to relate changes in canopy reflectance of different plant communities to appropriate stress traits with newly trained SVR algorithms. Only then could UAS-acquired images be used to monitor other ground-hugging vegetation communities, such as Arctic tundra (Bratsch, Epstein, Buchhorn, Walker, & Landes, 2017). Such methods could also be useful for monitoring

global change driven greening/browning (Phoenix & Bjerke, 2016), shrub encroachments (Sturm, Racine, & Tape, 2001), changes in high altitude montane range plant communities (Pauli et al., 2012) or even the decline of biological soil crusts in deserts and semiarid locations (Belnap, 2003). While the stress traits Cab and ELD are appropriate for many short stature plant communities, other estimates of canopy density, such as leaf area index (LAI) or colony mass per area (Waite & Sack, 2010) may be more suitable for complex canopy architectures. Moreover, Cab is not the most suitable indicator for use with epilithic moss and lichen communities characterized by photoprotective pigments that effectively mask optical signals of chlorophylls. Further investigations of the unique spectral characteristics of these communities might, however, enable their future methodological inclusion. Application to structurally complex terrestrial vegetation, for instance rangelands, woodlands and forests, requires a specific three-dimensional upscaling mechanism, which takes into account the spectral and geometrical properties of the canopy components such as optical properties and density of trunks, angularity of branches, clumping and angularity of leaves, etc. Modern approaches, facilitating this leaf-to-canopy spectral and structural upscaling, use so-called canopy radiative transfer models (Widlowski et al., 2015). These graphically and computationally intensive algorithms simulate physical interactions of solar irradiation, represented by photons or packets of photons, with biological material (i.e. plant foliage and wood) arranged in structurally representative canopy shapes (e.g. Gastellu-Etcheberry et al., 2015). Databases of air-/space-borne data, simulated by the canopy radiative transfer models, can be inverted to find quantitative inputs (Cab, LAI, etc.), which produce the best spectral agreement between modelled and real remote sensing observations (Malenovsky et al., 2013; Verrelst et al., 2015).

Finally, the approach presented here has the potential to be coupled with other complementary UAS remote sensing techniques, such as thermal mapping of plant foliage surface temperature (Turner, Barrand, et al., 2014; Turner, Lucieer, Malenovsky, King, & Robinson, 2014) and/or spectral sensing of photosynthesis-related chlorophyll fluorescence emissions (Malenovsky, Mishra, Zemek, Rascher, & Nedbal, 2009). Combination of these novel remote sensing techniques opens up new opportunities for detailed monitoring of important vegetation processes, for instance carbon assimilation and gross primary production, which are highly relevant for comprehensive understanding of global cycles and many types of environmental change.

### ACKNOWLEDGEMENTS

This study was funded by Discovery grant (DP110101714) from the Australian Research Council and Australian Antarctic Science grants (4046 and 4361). The Australian Antarctic Division (AAD) is acknowledged for fieldwork support and purchase of WorldView-2 images. DigitalGlobe, Inc. provided spectral response functions of the WorldView-2 sensor. The MODIS water vapour product was obtained from the Distributed Active Archive Center of the NASA GSFC, USA. Diana King was in receipt of an Australian Postgraduate Award. We thank Darren Turner and Tony Veness (University of Tasmania)

for supporting the unmanned aircraft operations and Anna Nydahl, Jessica Bramley-Alves, Rebecca Miller and Michael Ashcroft (all University of Wollongong) for field and laboratory assistance. Jane Wasley (University of Wollongong, AAD) was involved in designing the moss monitoring study and Matt King (University of Tasmania) provided helpful advice on the manuscript.

## AUTHORS' CONTRIBUTIONS

Z.M. designed the study, performed field, laboratory and airborne measurements and analyzed data; A.L. conducted field and airborne acquisitions and processed remote sensing data; S.A.R., J.D.T. and D.K. designed the long-term moss monitoring study; D.K. analyzed field monitoring data; J.D.T. conducted field and laboratory measurements of moss samples; S.A.R. conducted field measurements and led the ARC Discovery project. All authors co-wrote the paper.

## DATA ACCESSIBILITY

The following datasets, publicly available at the Australian Antarctic Data Centre (AADC) for data management and spatial data services ([https://data.aad.gov.au/metadata/records/AAS\\_4046\\_spectroscopy\\_chlorophyll/](https://data.aad.gov.au/metadata/records/AAS_4046_spectroscopy_chlorophyll/); <https://doi.org/10.4225/15/592f76a1045b0>), were used to conduct this study: (1) UAS hyperspectral images in reflectance, mask of moribund moss, airborne training and testing sets for the SVR machine learning, UAS maps of stress indicators and relative moss vigour at both study sites, (2) the WorldView-2 satellite reflectance data of investigated moss beds, space-borne training and testing sets for the SVR machine learning, satellite maps of stress indicators and relative moss vigour at both study sites, and (3) the 2013 ground validation data for 13 moss monitoring quadrats together with vector files delineating their geographical positions and orientations. Detailed information about collection and processing of ground moss health monitoring data can be obtained from University of Wollongong, Centre for Sustainable Ecosystem Solutions, School of Biological Sciences, Northfields Avenue, Wollongong, NSW 2522, Australia (contact Sharon Robinson: [sharonr@uow.edu.au](mailto:sharonr@uow.edu.au)).

## REFERENCES

- Aasen, H., Burkart, A., Bolten, A., & Bareth, G. (2015). Generating 3D hyperspectral information with lightweight UAV snapshot cameras for vegetation monitoring: From camera calibration to quality assurance. *ISPRS Journal of Photogrammetry and Remote Sensing*, 108, 245–259.
- Ač, A., Malenovský, Z., Hanuš, J., Tomášková, I., Urban, O., & Marek, M. V. (2009). Near-distance imaging spectroscopy investigating chlorophyll fluorescence and photosynthetic activity of grassland in the daily course. *Functional Plant Biology*, 36, 1006–1015.
- Anderson, K., & Gaston, K. J. (2013). Lightweight unmanned aerial vehicles will revolutionize spatial ecology. *Frontiers in Ecology and the Environment*, 11, 138–146.
- Asner, G. P., Brodrick, P. G., Anderson, C. B., Vaughn, N., Knapp, D. E., & Martin, R. E. (2016). Progressive forest canopy water loss during the 2012–2015 California drought. *Proceeding of the National Academy of Sciences of the United States of America*, 113, E249–E255.
- Asner, G. P., Martin, R. E., Knapp, D. E., Tupayachi, R., Anderson, C. B., Sinca, F., ... Llacayo, W. (2017). Airborne laser-guided imaging spectroscopy to map forest trait diversity and guide conservation. *Science*, 355, 385–389.
- Australian Antarctic Data Centre. (2009). State of Environment: Indicator 72—Windmill Islands terrestrial vegetation dynamics. Data management and spatial data services. Retrieved from [https://data.aad.gov.au/aadc/soe/display\\_indicator.cfm?soe\\_id=72](https://data.aad.gov.au/aadc/soe/display_indicator.cfm?soe_id=72) Accessed 2 June 2017.
- Belgiu, M., & Drăguț, L. (2016). Random forest in remote sensing: A review of applications and future directions. *ISPRS Journal of Photogrammetry and Remote Sensing*, 114, 24–31.
- Belnap, J. (2003). The world at your feet: Desert biological soil crusts. *Frontiers in Ecology and the Environment*, 1, 181–189.
- Brabyn, L., Green, A., Beard, C., & Seppelt, R. (2005). GIS goes nano: Vegetation studies in Victoria Land, Antarctica. *New Zealand Geographer*, 61, 139–147.
- Bramley-Alves, J., Wanek, W., French, K., & Robinson, S. A. (2015). Moss  $\delta^{13}\text{C}$ : An accurate proxy for past water environments in polar regions. *Global Change Biology*, 21, 2454–2464.
- Bratsch, S., Epstein, H., Buchhorn, M., Walker, D., & Landes, H. (2017). Relationships between hyperspectral data and components of vegetation biomass in Low Arctic tundra communities at Ivotuk, Alaska. *Environmental Research Letters*, 12, 025003.
- Bricher, P. K., Lucieer, A., Shaw, J., Terauds, A., & Bergstrom, D. M. (2013). Mapping sub-Antarctic cushion plants using random forests to combine very high resolution satellite imagery and terrain modelling. *PLoS ONE*, 8, e72093.
- Clarke, L. J., & Robinson, S. A. (2008). Cell wall-bound UV-screening pigments explain the high ultraviolet tolerance of the Antarctic moss, *Ceratodon purpureus*. *New Phytologist*, 179, 776–783.
- Clarke, L. J., Robinson, S. A., Hua, Q., Ayre, D. J., & Fink, D. (2012). Radiocarbon bomb spike reveals biological effects of Antarctic climate change. *Global Change Biology*, 18, 301–310.
- Colomina, I., & Molina, P. (2014). Unmanned aerial systems for photogrammetry and remote sensing: A review. *ISPRS Journal of Photogrammetry and Remote Sensing*, 92, 79–97.
- Convey, P., Bindenschadler, R., di Prisco, G., Fahrback, E., Gutt, J., Hodgson, D. A., ... Turner, J. (2009). Antarctic climate change and the environment. *Antarctic Science*, 21, 541–563.
- Convey, P., Chown, S. L., Clarke, A., Barnes, D. K. A., Bokhorst, S., Cummings, V., ... Wall, D. H. (2014). The spatial structure of Antarctic biodiversity. *Ecological Monographs*, 84, 203–244.
- Cracknell, A. P. (2017). UAVs: Regulations and law enforcement. *International Journal of Remote Sensing*, 38, 3054–3067.
- Cunliffe, A. M., Anderson, K., DeBell, L., & Duffy, J. P. (2017). A UK Civil Aviation Authority (CAA)-approved operations manual for safe deployment of lightweight drones in research. *International Journal of Remote Sensing*, 38, 2737–2744.
- Drăguț, L., Tiede, D., & Levick, S. R. (2010). ESP: A tool to estimate scale parameter for multiresolution image segmentation of remotely sensed data. *International Journal of Geographical Information Science*, 24, 859–871.
- Gastellu-Etcheberry, J. P., Yin, T., Lauret, N., Cajgfinger, T., Gregoire, T., Lopes, M., ... Ristorcelli, T. (2015). Discrete anisotropic radiative transfer (DART 5) for modelling airborne and satellite spectroradiometer and LIDAR acquisitions of natural and urban landscapes. *Remote Sensing*, 7, 1667–1701.
- Guglielmin, M., Fratte, M. D., & Cannone, N. (2014). Permafrost warming and vegetation changes in continental Antarctica. *Environmental Research Letters*, 9, 045001.
- Haboudane, D., Miller, J. R., Pattey, E., Zarco-Tejada, P. J., & Strachan, I. B. (2004). Hyperspectral vegetation indices and novel algorithms for predicting green LAI of crop canopies: Modeling and validation in the context of precision agriculture. *Remote Sensing of Environment*, 90, 337–352.



- Hodgson, J. C., & Koh, L. P. (2016). Best practice for minimising unmanned aerial vehicle disturbance to wildlife in biological field research. *Current Biology*, 26, 404–405.
- Horler, D. N. H., Dockray, M., Barber, J., & Barringer, A. R. (1983). Red edge measurement for remotely sensing plant chlorophyll content. *Advances in Space Research*, 3, 273–277.
- Jackson, R. D., & Huete, A. R. (1991). Interpreting vegetation indices. *Preventive Veterinary Medicine*, 11, 185–200.
- Kampe, T. U., Johnson, B. R., Kuester, M. A., & Keller, M. (2010). NEON: The first continental-scale ecological observatory with airborne remote sensing of vegetation canopy biochemistry and structure. *Journal of Applied Remote Sensing*, 4, art. no. 043510.
- Lary, D. J., Alavi, A. H., Gandomi, A. H., & Walker, A. L. (2016). Machine learning in geosciences and remote sensing. *Geoscience Frontiers*, 7, 3–10.
- Liu, N., & Treitz, P. (2016). Modelling high arctic percent vegetation cover using field digital images and high resolution satellite data. *International Journal of Applied Earth Observation and Geoinformation*, 25, 445–456.
- Lovelock, C. E., Jackson, A. E., Melick, D. R., & Seppelt, R. D. (1995). Reversible photoinhibition in Antarctic moss during freezing and thawing. *Plant Physiology*, 109, 955–961.
- Lovelock, C. E., & Robinson, S. A. (2002). Surface reflectance properties of Antarctic moss and their relationship to plant species, pigment composition and photosynthetic function. *Plant Cell and Environment*, 25, 1239–1250.
- Lucieer, A., Malenovský, Z., Veness, T., & Wallace, L. (2014). HyperUAS—Imaging spectroscopy from a multi-rotor unmanned aircraft system. *Journal of Field Robotics*, 31, 571–590.
- Lucieer, A., Turner, D., King, D. H., & Robinson, S. A. (2014). Using an unmanned aerial vehicle (UAV) to capture micro-topography of Antarctic moss beds. *International Journal of Applied Earth Observation and Geoinformation*, 27, 53–62.
- Malenovský, Z., Bartholomeus, H. M., Acerbi-Junior, F. W., Schopfer, J. T., Painter, T. H., Epema, G. F., & Bregt, A. K. (2007). Scaling dimensions in spectroscopy of soil and vegetation. *International Journal of Applied Earth Observation and Geoinformation*, 9, 137–164.
- Malenovský, Z., Homolová, L., Zurita-Milla, R., Lukeš, P., Kaplan, V., Hanuš, J., ... Schaepman, M. E. (2013). Retrieval of spruce leaf chlorophyll content from airborne image data using continuum removal and radiative transfer. *Remote Sensing of Environment*, 131, 85–102.
- Malenovský, Z., Mishra, K. B., Zemek, F., Rascher, U., & Nedbal, L. (2009). Scientific and technical challenges in remote sensing of plant canopy reflectance and fluorescence. *Journal of Experimental Botany*, 60, 2987–3004.
- Malenovský, Z., Turnbull, J. D., Lucieer, A., & Robinson, S. A. (2015). Antarctic moss stress assessment based on chlorophyll, water content, and leaf density retrieved from imaging spectroscopy data. *New Phytologist*, 208, 608–624.
- Mountrakis, G., Im, J., & Ogole, C. (2011). Support vector machines in remote sensing: A review. *ISPRS Journal of Photogrammetry and Remote Sensing*, 66, 247–259.
- Myneni, R. B., Hall, F. G., Sellers, P. J., & Marshak, A. (1995). The interpretation of spectral vegetation indexes. *IEEE Transactions on Geoscience and Remote Sensing*, 33, 481–486.
- Newsham, K. K., & Robinson, S. A. (2009). Responses of plants in polar regions to UV-B radiation: A meta-analysis. *Global Change Biology*, 15, 2574–2589.
- Pajares, G. (2015). Overview and current status of remote sensing applications based on unmanned aerial vehicles (UAVs). *Photogrammetric Engineering & Remote Sensing*, 81, 281–329.
- Pauli, H., Gottfried, M., Dullinger, S., Abdaladze, O., Akhalkatsi, M., Alonso, J. L. B., ... Grabherr, G. (2012). Recent plant diversity changes on Europe's mountain summits. *Science*, 336, 353–355.
- Phoenix, G. K., & Bjerke, J. W. (2016). Arctic browning: Extreme events and trends reversing arctic greening. *Global Change Biology*, 22, 2960–2962.
- Potters, G., Pasternak, T. P., Guisez, Y., & Jansen, M. A. K. (2009). Different stresses, similar morphogenic responses: Integrating a plethora of pathways. *Plant Cell and Environment*, 32, 158–169.
- Pottier, J., Malenovský, Z., Psomas, A., Homolová, L., Schaepman, M. E., Choler, P., ... Zimmermann, N. E. (2014). Modelling plant species distribution in alpine grasslands using airborne imaging spectroscopy. *Biology Letters*, 10, 20140347.
- Robinson, S. A., & Erickson, D. J. III (2015). Not just about sunburn—the ozone hole's profound effect on climate has significant implications for Southern Hemisphere ecosystems. *Global Change Biology*, 21, 512–527.
- Robinson, S. A., Turnbull, J. D., & Lovelock, C. E. (2005). Impact of changes in natural UV radiation on pigment composition, surface reflectance and photosynthetic function of the Antarctic moss, *Grimmia antarctici*. *Global Change Biology*, 11, 476–489.
- Royles, J., Amesbury, M. J., Convey, P., Griffiths, H., Hodgson, D. A., Leng, M. J., & Charman, D. J. (2013). Plants and soil microbes respond to recent warming on the Antarctic Peninsula. *Current Biology*, 23, 1702–1706.
- Shin, J. I., Kim, H. C., Kim, S. I., & Hong, S. G. (2014). Vegetation abundance on the Barton Peninsula, Antarctica: Estimation from high-resolution satellite images. *Polar Biology*, 37, 1579–1588.
- Skidmore, A. K., Pettorelli, N., Coops, N. C., Geller, G. N., Hansen, M., Lucas, R., ... Wegmann, M. (2015). Environmental science: Agree on biodiversity metrics to track from space. *Nature*, 523, 403–405.
- Smola, A. J., & Schölkopf, B. H. (2004). A tutorial on support vector regression. *Statistics and Computing*, 14, 199–222.
- Sturm, M., Racine, C., & Tape, K. (2001). Increasing shrub abundance in the Arctic. *Nature*, 411, 546–547.
- Tucker, C. J. (1979). Red and photographic infrared linear combinations for monitoring vegetation. *Remote Sensing of Environment*, 8, 127–150.
- Turnbull, J. D., & Robinson, S. A. (2009). Accumulation of DNA damage in Antarctic mosses: Correlations with ultraviolet-B radiation, temperature and turf water content vary among species. *Global Change Biology*, 15, 319–329.
- Turner, J., Barrand, N. E., Bracegirdle, T. J., Convey, P., Hodgson, D. A., Jarvis, M., ... Klepikov, A. (2014). Antarctic climate change and the environment: An update. *Polar Record*, 50, 237–259.
- Turner, D., Lucieer, A., Malenovský, Z., King, D. H., & Robinson, S. A. (2014). Spatial co-registration of ultra-high resolution visible, multispectral and thermal images acquired with Micro-UAV over Antarctic moss beds. *Remote Sensing*, 6, 4003–4024.
- Üstün, B., Melssen, W. J., & Buydens, L. M. (2007). Visualisation and interpretation of support vector regression models. *Analytica Chimica Acta*, 595, 299–309.
- Verrelst, J., Camps-Valls, G., Muñoz-Marí, J., Rivera, J. P., Veroustraete, F., Clevers, J. G. P. W., & Moreno, J. (2015). Optical remote sensing and the retrieval of terrestrial vegetation bio-geophysical properties—A review. *ISPRS Journal of Photogrammetry and Remote Sensing*, 108, 273–290.
- Vogelmann, J. E., Rock, B. N., & Moss, D. M. (1993). Red edge spectral measurements from sugar maple leaves. *International Journal of Remote Sensing*, 14, 1563–1575.
- Waite, M., & Sack, L. (2010). How does moss photosynthesis relate to leaf and canopy structure? Trait relationships for 10 Hawaiian species of contrasting light habitats. *New Phytologist*, 185, 156–172.
- Wasley, J., Robinson, S. A., Lovelock, C. E., & Popp, M. (2006). Some like it wet—biological characteristics underpinning tolerance of extreme water events in Antarctic bryophytes. *Functional Plant Biology*, 33, 443–455.
- Wasley, J., Robinson, S. A., Turnbull, J. D., King, D. H., Wanek, W., & Popp, M. (2012). Bryophyte species composition over moisture gradients in the Windmill Islands, East Antarctica: Development of a baseline for monitoring climate change impacts. *Biodiversity*, 13, 257–264.
- Widłowski, J. L., Mio, C., Disney, M., Adams, J., Andredakis, I., Atzberger, C., ... Zenone, T. (2015). The fourth phase of the radiative transfer model intercomparison (RAMI) exercise: Actual canopy scenarios and conformity testing. *Remote Sensing of Environment*, 169, 418–437.

Willmott, C. J. (1981). On the validation of models. *Physical Geography*, 2, 184–194.

## SUPPORTING INFORMATION

Additional Supporting Information may be found online in the supporting information tab for this article.

**How to cite this article:** Malenovský Z, Lucieer A, King DH, Turnbull JD, Robinson SA. Unmanned aircraft system advances health mapping of fragile polar vegetation. *Methods Ecol Evol.* 2017;8:1842–1857. <https://doi.org/10.1111/2041-210X.12833>